Observational signatures of outside-in accretion bursts in embedded protostars

August T. Masley, 1,2 Lee Hartmann 1

- ¹Department of Astronomy, University of Michigan, 1085 South University Avenue, Ann Arbor, MI 48015, USA
- ²Ritter Astrophysical Research Center, Department of Physics and Astronomy, University of Toledo, Toledo, OH 43606, USA

Accepted XXX. Received YYY; in original form ZZZ

ABSTRACT

Optical and infrared surveys have detected increasing numbers of disc accretion outbursts in young stars. Some models of these FU Ori-type events predict that the outburst should start at near- to mid-infrared wavelengths before an optical rise is detected, and this lag between infrared and optical bursts has been observed in at least two systems. Detecting and characterizing infrared precursors can constrain the outburst trigger region, and thus help identify the mechanism producing the outburst. However, because FU Ori objects are generally young and usually embedded in dusty protostellar envelopes, it is not clear whether or how well such infrared precursors can be detected in the presence of strong envelope extinction. To explore this question, we combine time-dependent outburst models of the inner disc with an outer dusty disc and protostellar envelope, and calculate the resulting spectral energy distributions (SEDs) using the radiative transfer code RADMC3D. We find that, for envelope mass infall rates $\geq 10^{-5} M_{\odot} \text{ yr}^{-1} (r_c/30 \text{ au})^{-1/2}$, where r_c is a characteristic inner radius for the infalling envelope, the infrared precursor is only apparent in the SED when viewed along an outflow cavity. At other inclinations, the precursor is most easily distinguished with limited envelope extinction at infall rates $\leq 10^{-6} M_{\odot} \text{ yr}^{-1} (r_c/30 \text{ au})^{-1/2}$. We also show that far-infrared and submm/mm monitoring can enable the indirect detection of precursor evolution long before the optical outburst, emphasizing the potential of long-wavelength monitoring for studying the earliest stages of protostar formation.

Key words: accretion – stars: pre-main-sequence – radiative transfer

1 INTRODUCTION

The study of accretion variability in young stars is being increasingly seen as providing important clues to disc physics and further insight into the processes by which stars accumulate their masses (e.g, Fischer et al. 2023). Of special interest are FU Ori objects (Hartmann & Kenyon 1996), many of which exhibit some of the largest accretion outbursts. A common model for these bursts is thermal triggering of the magnetorotational instability (MRI) (Balbus & Hawley 1991), which results in a large increase in the local viscosity and/or angular momentum transport, and a corresponding increase in accretion (Armitage et al. 2001; Zhu et al. 2010a,b; Bae et al. 2013, 2014).

While some FU Ori outbursts may require initiation in the innermost disc (Bell & Lin 1994), models that reproduce rapid, large rises in optical light invoke triggering at radii ~ 0.1 – 1 au and subsequent propagation inward. This outside-in burst picture predicts the appearance of an infrared precursor before the optical outburst becomes evident, and this has been observed in some (relatively low-luminosity) systems (Hillenbrand et al. 2018; Szegedi-Elek et al. 2020). The detection of such infrared precursors and measurement of the lag timescales for the subsequent optical brightening, can provide important constraints on where the outbursts are initiated and how they propagate, which in turn are crucial to identify outburst mechanisms (Cleaver et al. 2023). Moreover, detection of infrared precursors can help identify new FU Ori objects (Contreras Peña et al. 2025).

However, as FU Ori objects are often embedded in their dusty

envelopes, a combination of extinction and thermal emission can make it difficult to identify an object in outburst. Fischer et al. (2024) explored how observations at protostellar envelopes at mid-infrared to sub-mm wavelengths could be used to identify outbursts in systems whose central regions are heavily obscured. Modeling the accretion bursts as increases in luminosity of the central star, Fischer et al. found that observations at mid- to far-infrared wavelengths provided the best estimates of changes in protostellar accretion rates.

Our purpose here is different, in that we focus the detectability of non-steady disc temperature distributions and outburst temporal evolution on spectral energy distributions (SEDs). We adopt onedimensional, time-dependent models of disc outbursts from the work of Cleaver et al. (2023) as input to radiative transfer models of protostellar systems with infalling envelopes to explore the sensitivity of the SEDs to different stages of outside-in accretion outbursts. The models assume that a large α viscosity occurs when the disc internal temperature exceeds ~ 1300 K, to simulate triggering of the magnetorotational instability (MRI) due to thermal ionization in an otherwise cold and inert disc (Armitage et al. 2001; Zhu et al. 2010a,b). The envelopes are irradiated by the accreting disc, in contrast to other treatments that often assume a spherical symmetry for the input radiation field. The initial signature of the outburst occurs appears at infrared wavelengths, with the optical outburst coming later. We find that this infrared precursor will be clearly detectable when observed along outflow cavities, but may not be apparent when observing through the extincting envelope, depending upon the mass

infall rate, detailed envelope geometry, and viewing inclination. However, even when the infrared peak is not detectable, monitoring light curves at mid- to far-infrared and submm/mm wavelengths can provide important constraints on outburst properties and mechanisms.

We discuss our methods in §2, and show our results in §3. The implications of our results along with comparisons with the work of Fischer et al. (2024) are explored in §4, and our conclusions are summarized in §5.

2 METHODS

2.1 Radiative transfer

We use the software package RADMC3D (Dullemond et al. 2012) to calculate the temperature structure and emergent spectrum of our disc + envelope models. RADMC3D can accurately return a self-consistent temperature distribution based on the Monte Carlo method of Bjorkman & Wood (2001). We make use of RADMC3D's ability to include multiple dust species, each with its own density distribution and opacity table. In addition, we use the "heat source" option to account for the radiation produced by our luminous outbursting disc, as described in §2.4.

2.2 Density distribution

The two main components of our model density distributions are an envelope and a disc. The envelope is described using the density distribution for a collapsing and rotating singular sphere (Terebey et al. 1984), with the inner region described by the solutions of Ulrich (1976) and Cassen & Moosman (1981),

$$\rho_{env} = \frac{\dot{M}}{4\pi (GMr^3)^{1/2}} \left(1 + \frac{\cos\theta}{\cos\theta_\circ} \right)^{-1/2} \left(\frac{\cos\theta}{\cos\theta_\circ} + \frac{2\cos^2\theta_\circ}{r/r_c} \right)^{-1}$$
(1)

Here \dot{M} is the infall rate, M is the central body's mass, r and θ are the radial distance and polar angle in spherical coordinates, θ_{\circ} is the polar angle of a given streamline at infinity, and r_c is the centrifugal radius of the envelope. By using the mass infall rate as a parameter, we specify the stellar mass to fix the density needed for the radiative transfer solution. To simulate an outflow cavity, we set the density to zero for streamlines with $\theta_{\circ} \leq \theta_{out}$. We take the asymptotic cavity opening angle to be $\theta_{out} = 35^{\circ}$ unless otherwise specified.

The inner and outer disc regions require different treatment because the temperature distribution at small radii is driven by the disc accretion, while the outer cold dusty disc is passively irradiated by the inner regions. At radii less than 10 AU, the disc is assumed to be geometrically thin and optically thick, with the radiative flux as a function of cylindrical radius taken from the 1-D time-dependent outburst models of Cleaver et al. (2023). The surface density Σ is kept constant for R < 10 au at a value chosen to be continuous with the outer disk density distribution. The reason for this is to limit the optical depth of the inner disc as discussed in 2.4. At larger radii the disc is assumed to have a radial surface density distribution with a truncated power law in cylindrical radius R used in many works. Here we specifically adopt

$$\Sigma(R) = \Sigma_0 \left(\frac{R}{R_0}\right)^{-1} \exp\left(-\frac{R}{R_T}\right). \tag{2}$$

(e.g., Hartmann et al. 1998). Similarly, a typical assumption of ver-

tical isothermality is used for the structure in the z direction,

$$\rho_{disc} = \rho_0(R) \exp\left(\frac{-z^2}{2H^2}\right),\tag{3}$$

where ρ_0 is the midplane density and H is the scale height. We assume a radial dependence of the scale height $H = H_0 (R/R_0)^{5/4}$ which implies a disc temperature $T \propto R^{-1/2}$. We do not iterate the disc temperature and vertical hydrostatic equilibrium for consistency, as our focus here is not on the geometrical disc structure. As in Han et al. (2023), the transition between the disc and envelope density distributions is set where the disc thermal pressure $P_{disc} = \rho_{disc} c_s^2$, matches the ram pressure of the infalling envelope, $\rho_{env} v_\theta^2$, where c_s is the sound speed and v_θ is the velocity component approximately perpendicular to the disc surface.

2.3 Dust opacities

We assume that two primary dust species, olivine silicates and graphite, are present in the envelope and outer disc, with compositions given by Draine & Lee (1984). The opacities for these grains are calculated using the Mie scattering methods of D'Alessio et al. (2001a), based on the values of Dorschner et al. (1995) and Draine & Lee (1984).

For the envelope, we use these dust opacities assuming the usual power law distribution of dust as a function of radius $N(a) \propto a^{-3.5}$, with a maximum size $a_{max} = 0.3 \,\mu\text{m}$ typical of interstellar medium diffuse regions. For the disc, we adopt $a_{max} = 1 \,\text{mm}$, to allow for the settling of large dust as required in many systems (D'Alessio et al. 2001b; Villenave et al. 2020).

2.4 Inner disc in outbursts

The temperature structure of the inner disc is taken from the time-dependent simulations computed by Cleaver et al. (2023). These one-dimensional models assume that the optically-thick disc is heated by an α viscosity which turns on smoothly between 1200 K to 1300 K, to simulate activation of the MRI by thermal ionization. The SEDs were calculated by summing up the flux at each radial annulus assuming blackbody radiation for regions where dust opacity dominates, and stellar atmosphere models when dust is sublimated and the dominant opacity is from the gas.

During outbursts the inner disc becomes the main source of radiation rather than the central star. We therefore used the internal heat source method of RADMC3D, which allows us to input values of viscous heating directly. We take the energy fluxes at each radius from the calculations of Cleaver et al. (2023) and inject that heating into two grid cells spanning the midplane. This method allows us to generate a central source of radiation that has a more appropriate angular distribution of emergent intensities than that of a spherical source (i.e., discs radiate preferentially perpendicular to their surface). It also results in a radiating source with a more realistic spatial distribution than if we assumed a central radiation source. The values of the heat flux at each disc radius were taken from the snapshots of the time-dependent outburst models (i.e., from the effective temperature distributions), which can differ drastically from that of a steady accretion disc.

In the heat source method, RADMC3D assumes that the opacity

 $^{^1}$ Some calculations have suggested lower activation temperatures $\sim 800-1000$ K (Desch & Turner 2015), but changing this parameter would have little effect on our findings.

Table 1. Model parameters

Model	Outburst type	Infall rate $(M_{\odot} \text{ yr}^{-1})$	r _c (au)	Cavity θ_{out}	Outburst age (yr)
1	none	10^{-5}	30	35°	none
2A	FU	10^{-5}	30	"	50
2B	"	10^{-5}	30	"	70
2B'	"	10^{-5}	30	10°	70
2C	"	10^{-5}	30	35°	85
2D	"	10^{-5}	30	"	100
3	"	10^{-6}	30	"	70
4A	"	10^{-5}	3	"	70
4B	"	10^{-5}	30	"	70
5A	Gaia	10^{-5}	30	"	0
5B	"	10^{-5}	30	"	3
5C	"	10^{-5}	30	"	5
5D	"	10^{-6}	30	"	0
5E	"	10^{-6}	30	"	3
5F	"	10^{-6}	30	"	5

Outburst type is either the strong, FU Ori-like outburst (FU) or the a weaker, Gaia 17bpi-like outburst (Gaia) cases from Cleaver et al. (2023).

is that of dust. The time-dependent outburst models of Cleaver et al. (2023) use gas and dust Rosseland mean opacities internally and stellar model atmospheres to compute the emergent spectra. As we do not use gaseous opacities for the inner disc, we must use some other prescription to compute the disc SED. Furthermore, because accretion rates in the outburst models can be very high (peak values of $10^{-4} M_{\odot} \text{ yr}^{-1}$), central temperatures in the inner disc at peak outburst can approach 5×10^4 K, due to both the large viscous heating and the large optical depths that trap the radiation (Figure 1). We quickly found that adopting typical dust opacities (ignoring sublimation) and surface densities from the time-dependent simulations similarly resulted in very high internal temperatures that RADMC3D had great difficulty in handling. We therefore limit the surface density within R < 10 AU and apply a so-called "gray opacity" (adopting a constant absorptive opacity of 0.1 g cm⁻²) while simultaneously ensuring sufficient optical depth (in excess of $\tau \sim 10$), to ensure the appropriate emission at the disc surface while limiting the central temperatures and the number of scatterings required for the energy to escape.

Adopting a gray, temperature-independent opacity results in each disc annulus at R < 10 au emitting as a blackbody, depending upon the local effective temperature. We therefore do not reproduce the detailed spectral features of the SEDs in Cleaver et al. (2023), but this is unimportant for the purposes of irradiating the envelope and outer disc, as our method reproduces the overall shape of the disc SEDs reasonably well.

3 RESULTS

3.1 Model parameters

We computed several radiative transfer models for the time evolution of two different outbursts. For models 2A - 4B we adopt the inner disc temperature distributions of the "FU Ori-like" model of Cleaver et al. (2023) which culminate in a large outburst with peak accretion rates $\sim 10^{-4} M_{\odot} \, \mathrm{yr}^{-1}$. To achieve such a large outburst, it was triggered with a temperature perturbation at the relatively large radius of 1 au; consequently, the accretion front takes many years to reach the innermost disk and result in a burst at optical wavelengths. We selected snapshots at t = 50, 70, 85, and $100 \, \mathrm{yr}$ after outburst

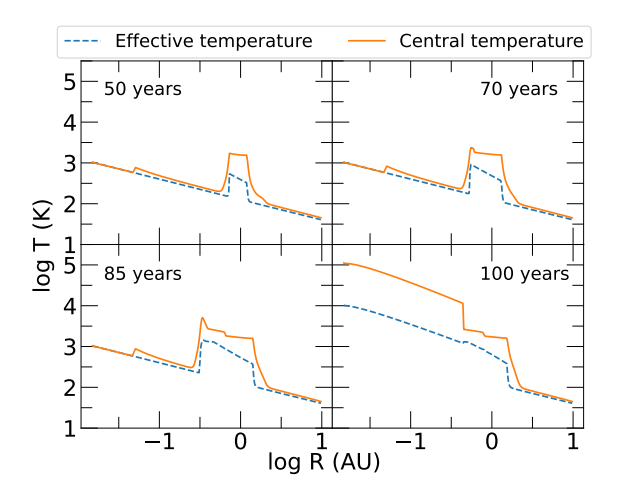


Figure 1. Evolution of the "large" (FU Ori-like) outburst model, showing the surface (effective) temperatures (blue dashed curves) and the central temperatures (orange solid curves), respectively, at four times after the initial triggering.

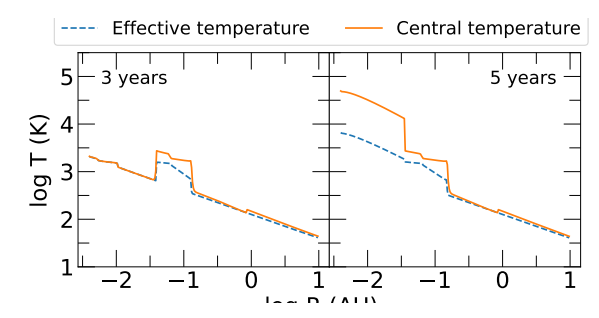


Figure 2. Evolution of the "small" (Gaia 17bpi-like) outburst model, showing the surface (effective) temperatures (blue dashed curve) and the central temperatures (orange solid curve), respectively, at two times after the initial triggering.

triggering for radiative transfer calculations (see Figure 1). This enables us to follow the evolution of the SED from precursor phases to a "final" phase in which the disc SED is essentially that of a standard steady-state, optically-thick disc.

The second set of model calculations take the disc temperature distributions from the simulations of Cleaver et al. (2023) modeling the smaller outburst of Gaia17bpi. This outburst was triggered at a smaller radius of 0.1 au, to achieve lower accretion rates and faster evolution. Two times are chosen; one just before the optical outburst at t=3 yr, and another at t=5 yr when the accretion rate was $4 \times 10^{-7} M_{\odot} \, \mathrm{yr}^{-1}$ (Figure 2).

We calculate envelope models for two mass infall rates: a 'high' infall rate of $1 \times 10^{-5} M_{\odot}/yr$, based upon the maximum of 'typical' rates of Zhu et al. (2009), and a lower rate of $1 \times 10^{-6} M_{\odot} \, \mathrm{yr}^{-1}$. (The important quantity for the radiative transfer solutions is the density structure, not the infall rate which depends upon the free-fall velocity. Our models thus correspond to true infall rates $\dot{M}(true) = \dot{M}(model)(M_*/M_{\odot})^{-1/2}$.) The envelope extends to a maximum radius of 6000 au, and we adopt an envelope outflow cavity within the streamline corresponding to $\theta_0 = 35^{\circ}$. These properties are typical of models for protostellar envelopes (see, e.g. Furlan et al. 2016). In all but one case we assume a centrifugal radius $r_c = 30$ au. This is based

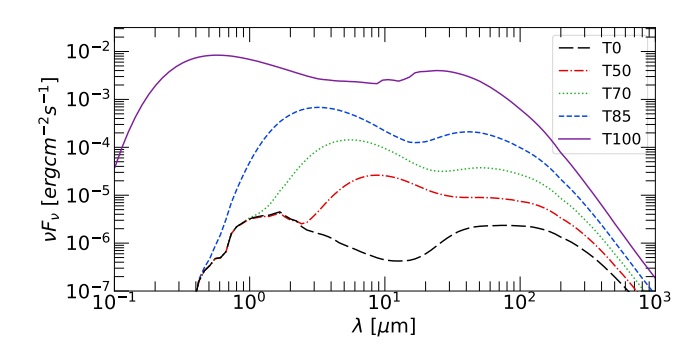


Figure 3. A comparison between the spectral energy distributions at an inclination of 0° for Model 1, with no outburst, Models and 2A - 2D of the FUor outburst sequence. The SED becomes brighter with increasing time.

on observations finding median protostellar disc radii $\sim 30-50$ au (Tobin et al. 2020).

For the central star we adopt a stellar spectrum with effective temperature of 3500 K and $\log g = 3$ from the BT-NextGen² models (Allard et al. 2011, 2012). We further adopt two sets of stellar parameters, one for each outburst type: a typical pre-main sequence stellar radius $R_* = 2R_{\odot}$ and a stellar mass $M_* = 0.44M_{\odot}$ in the case of the "FU Ori" model, and a smaller radius of $R_* = 0.8R_{\odot}$ and stellar mass $M_* = 0.2M_{\odot}$ for the Gaia 17bpi model. The mass only enters in setting the conversion from densities needed for the continuum radiative transfer to mass infall rates by changing the free-fall velocity (see above).

The disc parameters were the same for all cases: $R_0 = 10$ au, $R_T = 30$ au, and $\Sigma_0 = 750 \,\mathrm{g\,cm^2}$, with the fiducial disc scale height set to $H_0 = 0.809$ au at R_0 . The resulting disc mass is large $(0.16M_{\odot})$, consistent with the possibility of GI triggering of large outbursts (Cleaver et al. 2023, and references therein.).

Figure 1 shows four snapshots of the disc temperature structure from the FU Ori-like simulation. The viscous heating is triggered at ~ 1 au, and then the burst propagates inward as material accretes. Before the outburst reaches the inner disc, the central temperatures tend to thermostat at roughly 1500 K because we assume that dust is sublimated above that value (see discussion in Cleaver et al. 2023) and §4). When the outbursting region reaches the inner disc radii, dust is sublimated and the gas enters the gas opacity-dominated, thermally-unstable regime, causing temperatures to rise dramatically. In this stage the temperature distribution is essentially that of the standard steady, optically thick accretion disc, except that there is no turndown in T(R) at small radii because the simulations do not employ the zero-torque inner boundary condition (Shakura & Sunyaev 1973).

Figure 2 shows the temperature structure of the Gaia17bpi model disc at two times. In this case the outburst was triggered at a much smaller radius, 0.1 au, to make a better match of the calculated lag time between optical and infrared outburst signatures observed by Hillenbrand et al. (2018). The overall evolution is similar to that of the FU Ori-like models, except that it is much faster.

3.2 SEDs for FU Ori-like outburst

Fig. 3 shows the evolution of the SED for the FU Ori-like outburst, viewed at $i=0^{\circ}$ (down the cavity) to illustrate how the sequence of disc temperature distributions shown in Figure 1 affect the SEDs

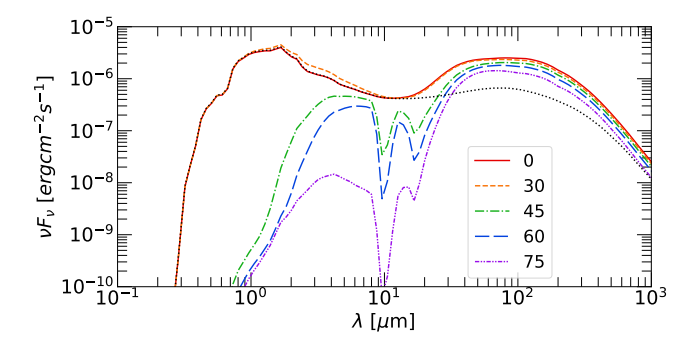


Figure 4. SEDs for Model 1 (star + disc + envelope), with an infall rate of $10^{-5} M_{\odot} \text{ yr}^{-1}$, with no outburst. The SEDs are fainter at higher inclination. The black dotted curve is the star and disc without envelope viewed at $i = 0^{\circ}$.

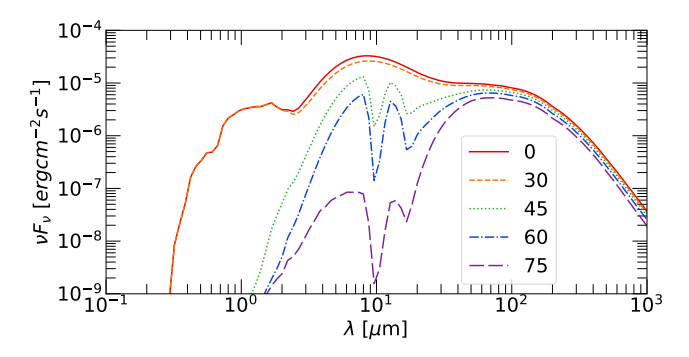


Figure 5. SEDs for Model 2A, with infall rate of $10^{-5}M_{\odot} \text{ yr}^{-1}$, $r_c = 30 \text{ au}$, at a time t = 50 yr after triggering. The infrared precursor produces a disc SED that peaks at around $8 - 10\mu\text{m}$.

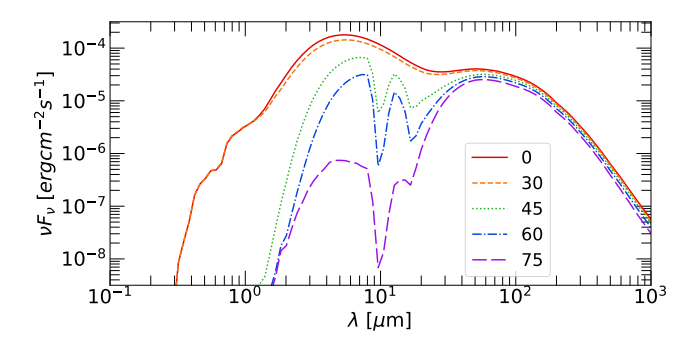


Figure 6. SEDs for Model 2B, with the outburst at t = 70 yr. Other parameters are the same as as Fig. 5. The precursor SED becomes brighter and bluer as the burst propagates inward.

without including envelope extinction. As the outside-in outburst progresses, the disc emission gets brighter and the peak of the SED gradually shifts to shorter wavelengths until the accretion front reaches the inner disc, at which point the disc becomes very much hotter and luminous. The mid- to far-infrared emission similarly becomes brighter and bluer as the outburst evolves (e.g., Furlan et al. 2016; Fischer et al. 2024).

Fig. 4 shows SEDs of Model 1 with only the star, envelope, and non-outbursting disc at different inclinations. This is intended to illustrate what the system would look like pre-outburst. At low inclinations, viewing the system through the cavity, the optical to mid-infrared spectrum of the system is clearly evident. The large far-infrared excess due to the envelope is only weakly dependent upon

http://svo2.cab.inta-csic.es/theory/newov2/index.php? models=bt-nextgen-agss2009

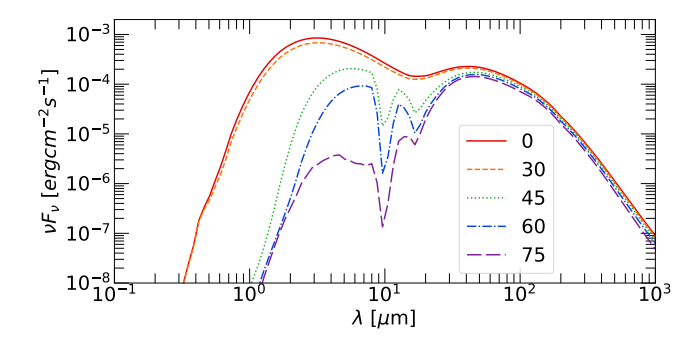


Figure 7. SEDs for Model 2C, with the outburst at t = 85 yr. Other parameters are the same as in Fig. 5.

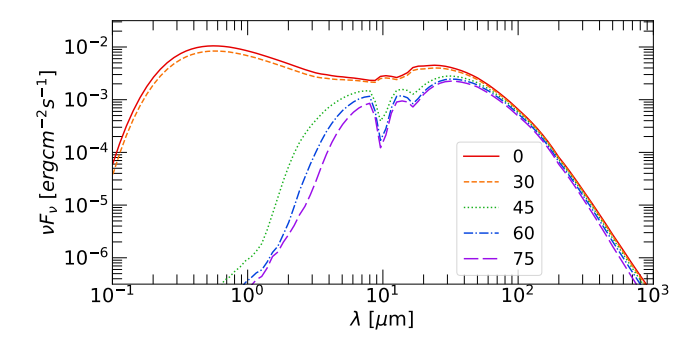


Figure 8. SEDs for Model 2D, with the outburst at t = 100 years. In this case the outburst has reached the inner disc, with much higher peak temperatures and luminosities. At this stage the disc SED is essentially that of a standard steady accretion model.

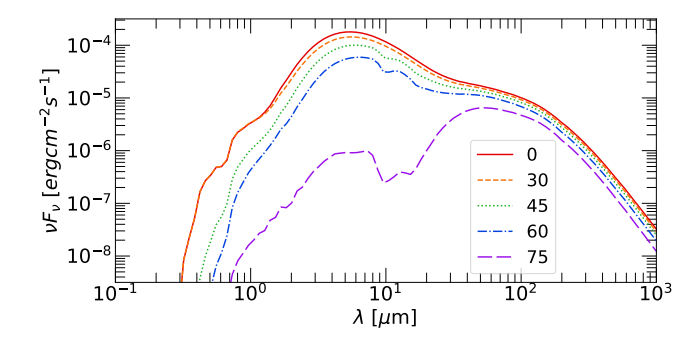


Figure 9. Spectral energy distributions for Model 3 (star + disc + envelope), at t = 70 yr with an infall rate of $10^{-6} M_{\odot} \text{ yr}^{-1}$ (Table 1).

inclination. Because we adopt a relatively geometrically-thick disc, the absorption features are due to a combination of disc and envelope extinction at $i = 75^{\circ}$. For reference, the black dotted curve shows the star plus disc without envelope viewed at $i = 0^{\circ}$.

Figures 5 through Fig. 8, models 2A - 2D, show the time evolution of the FUor-type outburst sequence for the envelope parameters of $\dot{M}=10^{-5}M_{\odot}~\rm yr^{-1}$ and $r_c=30$ au at different inclinations. In the following we use the term "infrared precursor" or simply "precursor" to refer to the increase in infrared kmission before the outburst is seen at optical wavelengths.

While the precursor is clearly evident when the system is viewed down the outflow cavity, its signature in the SED is much less evident if at all for higher inclinations. At $i = 45^{\circ}$ and $i = 60^{\circ}$ the emission at $\lambda \sim 5 - 10 \,\mu\text{m}$ (outside of the silicate absorption features) is

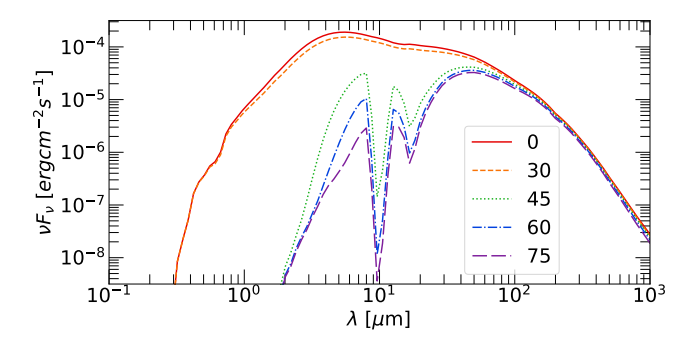


Figure 10. Spectral energy distributions for Model 4. This case is equivalent to Model 2B (Fig. 6), but with a much smaller centrifugal radius $r_c = 3$ au (see text).

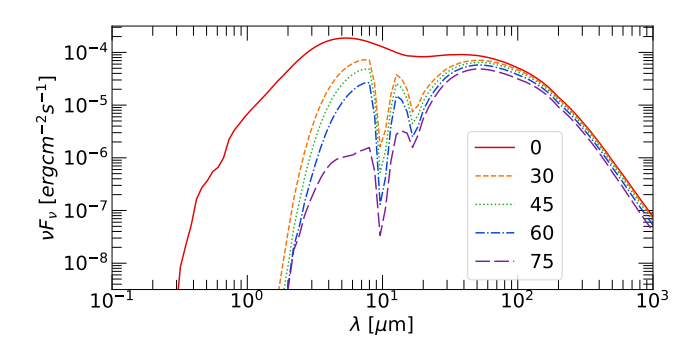


Figure 11. Spectral energy distributions for Model 2B', with the same parameters as Model 2B but with the cavity opening angle reduced from 35° to 10° (see text).

somewhat brighter than the far-infrared flux from $\sim 30-100\,\mu\mathrm{m}$, in contrast to typical protostellar SEDs, in which the $\sim 5-10\,\mu\mathrm{m}$ flux is fainter than the far-infrared emission (compare with 4; also Furlan et al. 2016 and Fischer et al. 2024). This inverted flux ratio might be a sign of the precursor, although it could be difficult to distinguish from an infrared companion (see futher discussion in §4.1). However, at $i=75^\circ$ the extinction due to the envelope and disc is too large to reveal any precursor emission.

Because the precursor emission peaks at $\sim 3-10\mu\text{m}$, it is not surprising that the amount of envelope extinction is crucial to identifying the early outburst in the SED. Figure 9 shows the outburst at t=70 yr, for the same parameters as model 2B (Figure 6, but for the lower infall rate of $10^{-6}M_{\odot}\text{ yr}^{-1}$). The precursor is clearly detectable at all but the highest inclinations due to the lower envelope extinction.

Conversely, envelope extinctions that are higher than in cases 2A-2D will make it very difficult to detect precursors unless viewed down the outflow cavity. The optical depth toward the central source in these envelope models scales approximately as $\tau \sim \dot{M} r_c^{-1/2}$ (see §4.1), so increasing this combined parameter will render any precursor undetectable. As an example, Figure 10 shows Model 4, with the same parameters as Model 2B except for a smaller centrifugal radius of 3 au. The increased extinction results in only a faint hint of the precursor at $i=45^\circ$ and none at higher inclinations.

The extinction toward the central source in these models also depends somewhat on our choice of outflow opening angle. This is because we define our cavities by the asymptotic angle θ_{out} of a streamline, which means that the infalling dusty mass lands on the disc at radii

$$r_{in} \ge \sin^2 \theta_{out} \, r_c \,. \tag{4}$$

6 A. T. Masley et al.

Figure 11 shows Model 2B', with the same parameters as Model 2B but changing θ_{out} from 35° to 10°. The extra extinction makes the precursor essentially undetectable, which is not surprising given that the inner edge of the infalling material at the disc has moved inward from 7.5 au to 0.9 au (equation 4). Note that this means some infalling material is landing on part of the outbursting region of the disc. Note also that for both the small r_c case (Figure 10) as well as this small opening angle case the near-infrared excess becomes undetectable unless viewed down the cavity.

This discussion only addresses the detection of the infrared precursor in the SED. However, the evolution of the precursor can be traced indirectly through the overall increase in the system luminosity as the outburst propagates inward, even at high line-of-sight extinctions. We address the time variability as a function of the wavelength of observation in §4.

3.3 SEDs for Gaia 17bpi outburst

The other outburst case we consider uses the models of Cleaver et al. (2023) for Gaia 17bpi, which exhibited a much smaller outburst than the FU Ori case, $\sim 1-6\times 10^{-7}M_{\odot}\,\mathrm{yr^{-1}}$ (Hillenbrand et al. 2018; Rodriguez & Hillenbrand 2022). Such smaller outbursts are more common than the large FUor bursts (e.g., Fischer et al. 2023; Contreras Peña et al. 2024), so we use these models to evaluate the detectability of these less powerful, shorter timescale events.

The models for Gaia 17bpi by Cleaver et al. (2023) assumed that the outburst was triggered at radius of 0.1 au, compared with the 1 au triggering of the FU Ori-like outburst (Figure 1). This difference results in much faster evolution and a much shorter time lag between the infrared precursor and the optical outburst. Because the accretion front does not have far to propagate inwards before maximum light, the precursor is only seen as a peak in the SED at $\sim 2 - 3 \,\mu\text{m}$ about two years before the SED becomes that of a steady accretion disc, as shown in the i=0 sequence in Figure 12.

The lower panel of Figure 12 shows that the precursor is not detectable for $i = 60^{\circ}$ at $10^{-5} M_{\odot} \, \mathrm{yr}^{-1}$ and $r_c = 30$ au. Unlike Model 2B, the precursor emission is considerably redder, where the extinction is larger. For the lower infall rate of $10^{-6} M_{\odot} \, \mathrm{yr}^{-1}$, the precursor is detectable at $i = 60^{\circ}$ (Figure 13), but it would be difficult to differentiate the source spectrum from a steady disc with a lower maximum temperature.

4 DISCUSSION

4.1 Detectability and evolution of outburst

The outburst simulations predict that during the precursor phase, before the optical rise, the disc SEDs exhibit a peak in the $2-10~\mu m$ region, indicating that the temperature of the hot region of the disc is around $\approx 1000~K$. There are two reasons for this. One is the choice of our trigger central temperature of $\sim 1300~K$, with a somewhat lower surface or effective temperature. The trigger temperature is particularly important for low, inner disk outbursts such as those of Gaia17bpi, because the burst does not propagate very far inward before optical maximum light.

For large, long-lasting outbursts such as the FU Ori-type case, another effect is more important for the evolution of the precursor: the thermostatic effect caused by the assumed sublimation of dust at $T \sim 1500$ K. The central temperature in the hot region is maintained by viscous dissipation with radiative trapping that results in a higher central temperature than at the surface. If the temperature rises above

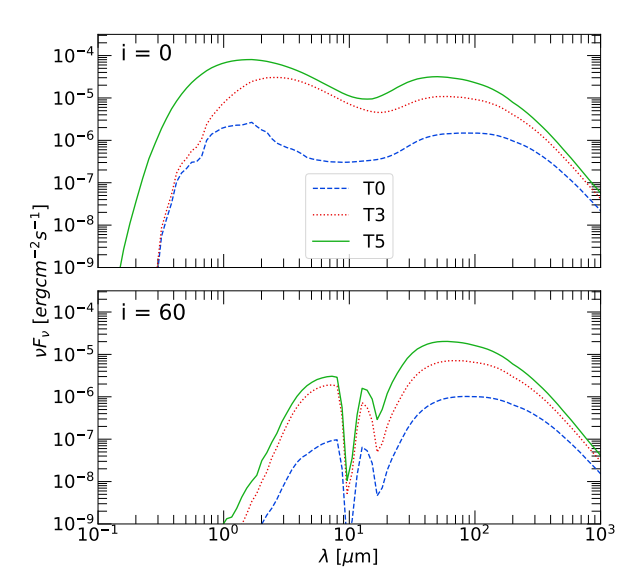


Figure 12. Spectral energy distributions for Models 5A - 5C of the Gaia outburst. Three times are compared, at 0, 3, and 5 years, corresponding to a non-outbursting, precursor, and peak outburst. The upper panel compares the three at a 0-degree inclination, while the lower compares the three at a 60-degree inclination.

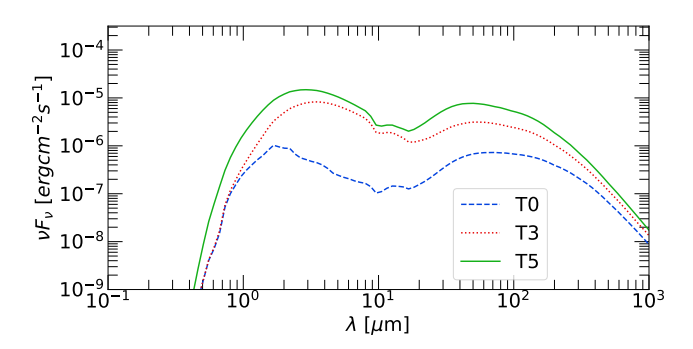


Figure 13. SEDs for the Gaia disc outburst case but with $\dot{M} = 10^{-6} M_{\odot} \text{ yr}^{-1}$ (Models 5D,E,F), observed at an inclination of $i = 60^{\circ}$.

1500 K, the disappearance of dust results in a large decrease in the opacity - which then reduces the radiative trapping and cools the interior. The net effect of this thermostatic behavior is that the hot region's effective temperature remains very roughly at $\sim 1000~K$ during the precursor phase.

As the large burst propagates inward, the effective temperature of the hot region does not remain precisely constant but becomes somewhat hotter (Figure 1). This causes the SED peak to move from $\sim 10\,\mu\text{m}$ at early phases to $\sim 3\,\mu\text{m}$ as the overall outburst brightens (see Fig. 3). The SED only changes dramatically when the burst reaches small radii. At this point the viscous heating becomes too large for dust to survive, and the dependence of the gas opacity on temperature triggers a thermal instability resulting in much higher temperatures (Fig. 1, bottom right panel). In this phase the SED has essentially the shape of the standard steady, optically-thick accretion disc spectrum (Figure 8).

The envelope modifies the disc SEDs by both absorbing and

recemitting radiation from the central regions. Given that the peak temperature in the disc is $\sim 1000~\rm K$ for many years in the large outburst case, the precursor emission peak occurs at a wavelength where the envelope mostly absorbs. In these models the optical depth along a particular line of sight to the central regions scales as

$$\tau_{\lambda} \propto k_{\lambda} \dot{M} r_c^{-1/2} \,, \tag{5}$$

where k_{λ} is the opacity. As illustrated in our "base" case, with $\dot{M}=10^{-5}M_{\odot}\,\mathrm{yr}^{-1}$ and $r_c=30$ au, a hint of the disc SED peak is present at $i=45^{\circ}$ but not apparent at larger inclinations. For $\dot{M}=10^{-6}M_{\odot}\,\mathrm{yr}^{-1}$ and the same centrifugal radius, the reduction in envelope optical depth of a factor ~ 3 results in the disc SED peak being very detectable, except at the highest inclinations, where the disc absorption becomes dominant. Similarly, for $\dot{M}=10^{-5}M_{\odot}\,\mathrm{yr}^{-1}$ and $r_c=3$ au, the increase in optical depth prevents detection of the precursor SED peak.

The other effect of the envelope is to reradiate the central source emission at long wavelengths. For the larger values of centrifugal radius, and our chosen cavity properties, the far-infrared peak of the disc SED is well displaced in wavelength from the precursor peak (Models 2A-D). However, for model B', with $r_c=3$ au, the infalling dust extends much closer to the star and becomes much hotter, such that the envelope emission begins to merge in wavelength with that of the precursor as seen down the cavity. In this case the presence of the precursor SED peak may be difficult to identify with confidence.

Another possible problem in identifying an infrared precursor would be misidentification due to presence of an embedded binary companion that is only detected at infrared wavelengths. An example of this is the Z CMa system, which consists of an FU Ori object well-detected at optical wavelengths, with an infrared companion separated by only 0.1" that dominates the system luminosity (Koresko et al. 1991). The SED of the joint system is qualitatively similar to that of the fiducial model. Ruling out an infrared companion would require interferometry or possibly detection of the companion in scattered light (Whitney et al. 1993).

Obviously it is much easier to detect the outburst precursors predicted by these models when viewing along an outflow cavity. We have chosen a relatively large opening angle which may overestimate the probability of finding objects with favorable inclinations. Another potential problem is the presence of external extinction. In modelling the SEDs of Orion protostars, Furlan et al. (2016) inferred large external extinctions for many sources. Absorption of $A_V \gtrsim 10$ would obscure any potential precursor signal otherwise unaffected by envelope extinction.

Despite the dificulties of clearly detecting a precursor photometrically in highly extincted systems, observing the time evolution of long-wavelength emission could provide independent evidence of precursor outburst evolution. In an analysis of the Spitzer/IRAC Candidate YSO (SPICY) Catalog for variables in the inner galaxy (Kuhn et al. 2021), supplemented where possible with data from the VVV project (Smith et al. 2025), Contreras Peña et al. (2025) attempted to identify candidate FUors from slow, "linear" increases or decreases in light rather than the usual search for quick, largeamplitude bursts. These types of light curves could correspond to the slow decay phase of outburst, as seen in FU Ori (Herbig 1977), or a slow rise in accretion. The rising light curves could represent an inside-out burst (Bell & Lin 1994) as observed for V1515 Cyg (Herbig 1977). Alternatively, linear rising light curves might also be the signature of outside-in precursors. With spectroscopic followup of a small subsample, Contreras Peña et al. (2025) were able to confirm that genuine FUors are identifiable from these light curve classifications, potentially greatly expanding the census of outbursting young

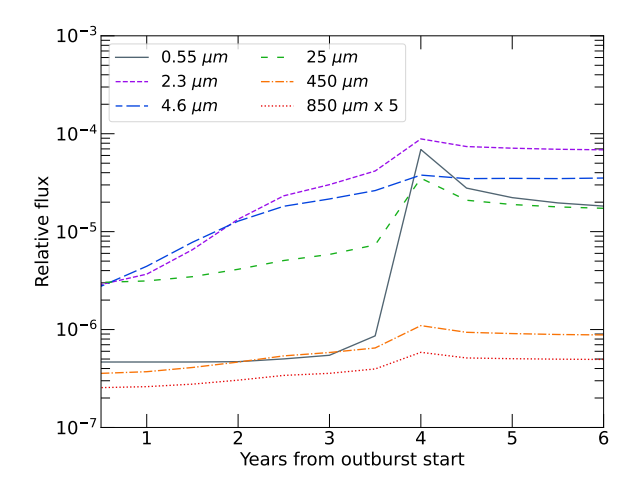


Figure 14. Light curves of relative flux for the Gaia-type outburst, demonstrating its time evolution for a variety of wavelengths. Note that the parameters are identical to Models 5A - 5C, observed at an inclination of 0° .

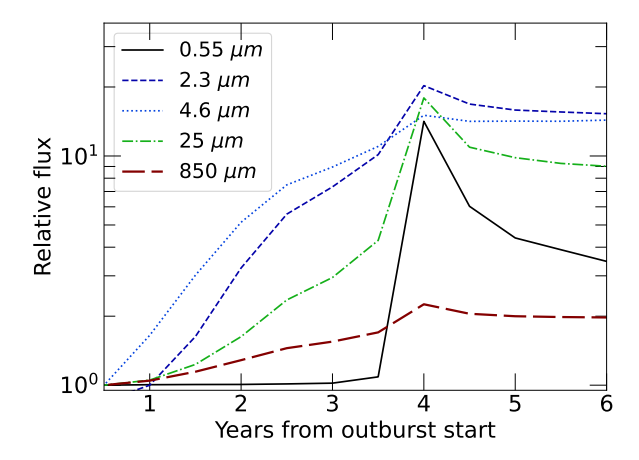


Figure 15. Flux evolution at five wavelengths for the Gaia17bpi outburst (Models 5D,E,F), observed through the envelope at a typical inclination of 60° , but now normalized to the flux in the pre-outburst state.

objects, and further observations of systems slowly rising in brightness could yield insights into burst triggering even without detailed SED signatures.

4.2 Comparison with prior work

The previous study most relevant for this work is that of Fischer et al. (2024), which explored the most favorable wavelength ranges to detect outbursts of highly extincted protostars. Their envelope and disc models were taken from the results of Furlan et al. (2016) for 86 Class 0 protostars in Orion. Fischer et al. computed SEDs for these models with increases in luminosity ranging from 10 to 100 times the original, and then analyzed the fractional changes at various wavelengths relative to the true change in luminosity. Consistent with earlier, more limited studies (Baek et al. 2020; MacFarlane et al. 2019; Contreras Peña et al. 2020), Fischer et al. concluded that far-infrared measurements most closely represented the intrinsic luminosity changes, and

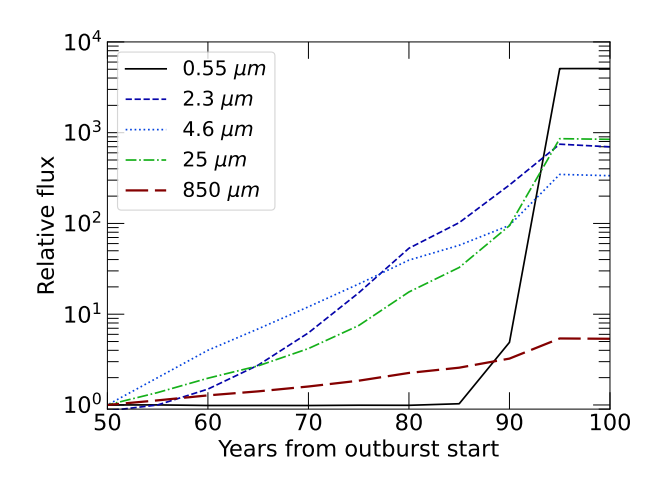


Figure 16. Evolution of the fluxes at the same five wavelengths as in Figure 15, but for the FU Ori-like outburst sequence (Models 2A,B,C,D), normalized to the flux at 50 years after initial triggering, and observed through the envelope at 60°.

that far-IR and longer wavelength observations were preferred over studies at shorter wavelengths strongly affected by extinction.

Our aim in this paper is different from Fischer et al. in that we consider detectability and time evolution of the infrared precursor predicted by models of outside-in bursts. As the signature of the model is a peak in disc emission in the $2-10\,\mu\mathrm{m}$ wavelength range, our focus is on detection at shorter wavelengths than those favored more generally by Fischer et al. In addition, we focus on the time evolution of the outburst. As shown in Figures 14 and 15, the precursor in the Gaia models is strongest at $4.6\,\mu\mathrm{m}$, whereas the $25\,\mu\mathrm{m}$ signal is somewhat smaller, and very weak in the submm region, as found by Fischer et al. (2024).

Qualitatively similar flux evolution is shown in Figure 16 for the FU Ori-like outburst; the main difference is that the increase in the fluxes is slower and ultimately larger. Contreras Peña et al. (2025) found potential FUors with "linear", slow rises in brightness at 3.4 μ m and 4.6 μ m (WISE W1 and W2 bands), increasing by $\sim 1-2$ magnitudes over ~ 10 yr. roughly consistent with the flux evolution shown in Figure 16. The rise timescale in the simulations is set by the location of the initial trigger and the adoption of a viscosity parameter $\alpha=0.1$. While the choice of α was set by matching burst evolution to observations of Gaia17bpi, it must be emphasized that full global magnetohydrodynamic simulations, which show much more complex behavior than can be captured with a one-dimensional, alpha viscosity treatment (e.g., Zhu et al. 2020; Roberts et al. 2025), are needed to make more robust predictions.

Once the outburst reaches peak luminosity, most of the radiation originates near the central protostar. Thus at this stage the simulations are only moderately different from the Fischer et al. treatment, which assumes that all the radiative energy originates from the central protostar with a fixed effective temperature, varying the protostellar radius to achieve differing system luminosities. Viewed down the outflow cavity, the SED of the disc will look different from the star, but at other inclinations and with high enough envelope/external extinction, the source spectrum will not matter as the system SED will be dominated by emission from the dusty envelope. Another difference is that while we use the same density structure as that of Furlan et al. (2016) (equation 1), we use a different cavity shape, which generally makes little difference to SEDs (although it is important

for modeling scattered light images). Finally, a disc has a different angular distribution of radiation than that of a spherical star (see Appendix), but this is likely of secondary importance considering other uncertainties in envelope and cavity structures.

Our results show that, for outside-in accretion bursts, near-infrared monitoring can be useful in detecting precursors except in the most heavily-extincted systems. In any case our simulations reinforce the conclusion of Fischer et al. (2024) that far-infrared and longer wavelengths can reliably detect outbursts in protostars. Because the youngest systems will be the most embedded, long-wavelength monitoring can probe the onset of outbursts in the earliest stages of protostar formation.

5 CONCLUSIONS

We have computed SEDs for protostars to explore the effects of infalling envelopes on the detectability of of outside-in accretion outbursts. Specifically, we consider models of outside-in propagation of accretion bursts that predict mid-infrared precursors that are in principle detectable before the optical light burst. We find that for envelope infall rates $\gtrsim 10^{-5} M_{\odot} \,\mathrm{yr}^{-1}$ to disk radii ~ 30 au, the peak of the precursor emission is difficult to discern due to high extinction unless the system is viewed down an outflow cavity. However, at more modest infall rates $\lesssim 10^{-6} M_{\odot} \,\mathrm{yr}^{-1}$, the mid-infrared peak is detectable, except at high inclinations where disc occultation/extinction is important. We find agreement with the results of Fischer et al. (2024) that mid-infrared studies are more sensitive to outbursts than submm and mm observations. However, in addition our outburst models predict that the $\sim 2-10 \,\mu m$ range is more sensitive to the outburst precursor. Monitoring at long wavelengths presents intriguing possibilities of of detecting precursor luminosity increases, particularly in the infrared (e.g., Contreras Peña et al. 2025), but even submm/mm monitoring can provide useful constraints. Detection of such precursors, and measurements of the lag time between infrared and optical bursts, can be important in constraining the radial distance at which the outburst starts (Cleaver et al. 2023). Our results may help inform observing strategies for improving the characterization of protostellar accretion.

ACKNOWLEDGEMENTS

We are extremely grateful to Jacob Cleaver and Fiona Han for allowing access to their work, as well as aiding us in its operation and understanding. We would also like to thank Cornelis Dullemond for answering our questions over correspondence, and Nuria Calvet for providing detailed opacity tables. LH was supported in part by NASA Emerging Worlds grant 80NSSC24K1285. Software: RADMC3D (Dullemond et al. 2012), SPECTRES (Carnall 2017), MATPLOTLIB (Hunter 2007).

DATA AVAILABILITY

The models and associated data will be provided upon reasonable request to the authors.

REFERENCES

Allard F., Homeier D., Freytag B., 2011, in Johns-Krull C., Browning M. K., West A. A., eds, Astronomical Society of the Pacific Conference Series

```
Vol. 448, 16th Cambridge Workshop on Cool Stars, Stellar Systems, and
    the Sun. p. 91 (arXiv:1011.5405)
Allard F., Homeier D., Freytag B., 2012, Philosophical Transactions of the
    Royal Society of London Series A, 370, 2765
Armitage P. J., Livio M., Pringle J. E., 2001, MNRAS, 324, 705
Bae J., Hartmann L., Zhu Z., Gammie C., 2013, ApJ, 764, 141
Bae J., Hartmann L., Zhu Z., Nelson R. P., 2014, ApJ, 795, 61
Baek G., et al., 2020, ApJ, 895, 27
Balbus S. A., Hawley J. F., 1991, ApJ, 376, 214
Bell K. R., Lin D. N. C., 1994, ApJ, 427, 987
Bjorkman J. E., Wood K., 2001, ApJ, 554, 615
Carnall A. C., 2017, SpectRes: A Fast Spectral Resampling Tool in Python
    (arXiv:1705.05165)
Cassen P., Moosman A., 1981, Icarus, 48, 353
Cleaver J., Hartmann L., Bae J., 2023, Monthly Notices of the Royal Astro-
    nomical Society, 523, 5522
Contreras Peña C., Johnstone D., Baek G., Herczeg G. J., Mairs S., Scholz
    A., Lee J.-E., JCMT Transient Team 2020, MNRAS, 495, 3614
Contreras Peña C., Lucas P. W., Guo Z., Smith L., 2024, MNRAS, 528, 1823
Contreras Peña C., et al., 2025, ApJ, 987, 23
D'Alessio P., Calvet N., Hartmann L., 2001a, ApJ, 553, 321
D'Alessio P., Calvet N., Hartmann L., 2001b, ApJ, 553, 321
Desch S. J., Turner N. J., 2015, ApJ, 811, 156
Dorschner J., Begemann B., Henning T., Jaeger C., Mutschke H., 1995, A&A,
    300, 503
Draine B. T., Lee H. M., 1984, ApJ, 285, 89
Dullemond C. P., Juhasz A., Pohl A., Sereshti F., Shetty R., Peters T., Com-
    mercon B., Flock M., 2012, RADMC-3D: A multi-purpose radiative
    transfer tool, Astrophysics Source Code Library, record ascl:1202.015
Fischer W. J., Hillenbrand L. A., Herczeg G. J., Johnstone D., Kospal A.,
    Dunham M. M., 2023, in Inutsuka S., Aikawa Y., Muto T., Tomida
    K., Tamura M., eds, Astronomical Society of the Pacific Conference
    Series Vol. 534, Protostars and Planets VII. p. 355 (arXiv: 2203.11257),
    doi:10.48550/arXiv.2203.11257
Fischer W. J., et al., 2024, AJ, 167, 82
Furlan E., et al., 2016, ApJS, 224, 5
Han F., Hartmann L., Calvet N., Franco-Hernández R., 2023, MNRAS, 526,
    2566
Hartmann L., Kenyon S. J., 1996, ARA&A, 34, 207
Hartmann L., Calvet N., Gullbring E., D'Alessio P., 1998, ApJ, 495, 385
Herbig G. H., 1977, ApJ, 217, 693
Hillenbrand L. A., et al., 2018, The Astrophysical Journal, 869, 146
Hunter J. D., 2007, Computing in Science & Engineering, 9, 90
Koresko C. D., Beckwith S. V. W., Ghez A. M., Matthews K., Neugebauer
    G., 1991, AJ, 102, 2073
Kuhn M. A., de Souza R. S., Krone-Martins A., Castro-Ginard A., Ishida E.
    E. O., Povich M. S., Hillenbrand L. A., COIN Collaboration 2021, ApJS,
    254, 33
MacFarlane B., Stamatellos D., Johnstone D., Herczeg G., Baek G., Chen
    H.-R. V., Kang S.-J., Lee J.-E., 2019, MNRAS, 487, 4465
Roberts M. J. O., Latter H. N., Lesur G., 2025, arXiv e-prints, p.
    arXiv:2506.16945
Rodriguez A. C., Hillenbrand L. A., 2022, The Astrophysical Journal, 927,
    144
Shakura N. I., Sunyaev R. A., 1973, A&A, 24, 337
Smith L. C., et al., 2025, MNRAS, 536, 3707
Szegedi-Elek E., et al., 2020, The Astrophysical Journal, 899, 130
Terebey S., Shu F. H., Cassen P., 1984, ApJ, 286, 529
Tobin J. J., et al., 2020, ApJ, 890, 130
Ulrich R. K., 1976, ApJ, 210, 377
```

Villenave M., et al., 2020, A&A, 642, A164

L., Kenyon S. J., 1993, ApJ, 417, 687

2010a, ApJ, 713, 1134

Yorke H. W., Bodenheimer P., 1999, ApJ, 525, 330 Zhu Z., Hartmann L., Gammie C., 2009, ApJ, 694, 1045

Whitney B. A., Clayton G. C., Schulte-Ladbeck R. E., Calvet N., Hartmann

Whitney B. A., Wood K., Bjorkman J. E., Wolff M. J., 2003, ApJ, 591, 1049

Zhu Z., Hartmann L., Gammie C. F., Book L. G., Simon J. B., Engelhard E.,

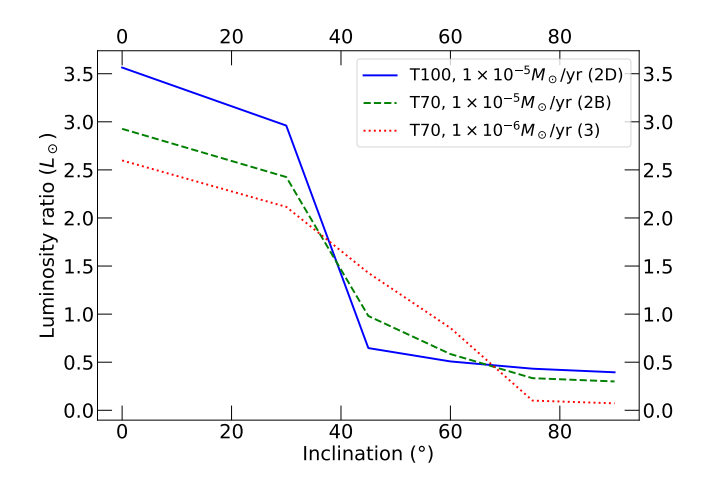


Figure A1. The inclination dependence of luminosity for Models 2B, 2D, and 3, including full stellar, disc, and envelope components. The flashlight effect is clearly apparent, as is its dependence on envelope infall rate.

Zhu Z., Hartmann L., Gammie C., 2010b, ApJ, 713, 1143 Zhu Z., Jiang Y.-F., Stone J. M., 2020, MNRAS, 495, 3494

APPENDIX A: INCLINATION-DEPENDENT APPARENT LUMINOSITY

The radiation from discs is anisotropic; in addition, protostellar envelopes generally are not spherical, which can cause important variations in spectral appearance as a function of inclination. Whitney et al. (2003) explored the effects of non-spherical geometry on the SEDs, images, and apparent luminosities of protostars. Their envelope models were essentially the same as ours but with somewhat different outflow cavity parameters. Whitney et al. found that pole-on viewing angles might result in overestimating true source luminosities by a factor ~ 2 due to the "flashlight effect" (Yorke & Bodenheimer 1999), with the envelope geometry in effect channelling radiation out lower extinction regions. Conversely, Whitney et al. found that more edge-on systems might appear underluminous by a factor of 1.5 (or more if occulted by the disc; see their Figure 10).

While Whitney et al. (2003) did include disc emission, most of the accretion luminosity arose from inside the dust destruction radius; and this radiation was assumed to come from the central star. As a result, the radiation from central regions in the Whitney et al. models is more spherically symmetric than in our calculations. As an example of the effect of the anisotropy of disc emission, in Figure A1 we show what the inferred luminosity would be relative to the true value for Models 2B, 2D, and 3). As expected, observations at low inclinations yield inferred luminosities brighter than the true value by factors \sim 3, higher than that found by Whitney et al. due to the anisotropy of disc emission. Conversely, as found by Whitney et al., objects viewed at a median inclinations, \sim 60°, will appear underluminous, by a factor of two or more.

This paper has been typeset from a $\ensuremath{\text{TEX/LATEX}}$ file prepared by the author.